ARTICLE

OPEN

Check for updates

The effect of turbulence in brain dynamics information transfer measured with magnetoencephalography

Gustavo Deco [1,2✉], Samuel Liebana Garcia[3], Yonatan Sanz Perl[1,4], Olaf Sporns[5,6,7,8] & Morten L. Kringelbach[9,10,11✉]

Fast, efficient information transfer is essential for the brain to ensure survival. As recently shown in functional magnetic resonance imaging with high spatial resolution, turbulence appears to offer a fundamental way to facilitate energy and information transfer across spatiotemporal scales in brain dynamics. However, given that this imaging modality is comparably slow and not directly linked with neuronal activity, here we investigated the existence of turbulence in fast whole-brain neural dynamics measured with magnetoence-phalography (MEG). The coarse spatial observations in MEG necessitated that we created and validated a empirical measure of turbulence. We found that the measure of edge-centric metastability perfectly detected turbulence in a ring of non-local coupled oscillators where the ground-truth was analytically known, even at a coarse spatial scale of observations. This allowed us to use this measure in the spatially coarse, empirical large-scale MEG data from 89 human participants. We demonstrated turbulence in fast neuronal dynamics and used this to quantify information transfer in the brain. The results demonstrate that the necessary efficiency of brain function is dependent on an underlying turbulent regime.

[1] Center for Brain and Cognition, Computational Neuroscience Group, Department of Information and Communication Technologies, Universitat Pompeu Fabra, Roc Boronat 138, Barcelona 08018, Spain. [2] Institució Catalana de la Recerca i Estudis Avançats (ICREA), Passeig Lluís Companys 23, Barcelona 08010, Spain. [3] Department of Physiology, Anatomy & Genetics, University of Oxford, Oxford, UK. [4] Department of Physics, University of Buenos Aires, Buenos Aires, Argentina. [5] Department of Psychological and Brain Sciences, Indiana University, Bloomington, IN, USA. [6] Cognitive Science Program, Indiana University, Bloomington, IN, USA. [7] Program in Neuroscience, Indiana University, Bloomington, IN, USA. [8] Network Science Institute, Indiana University, Bloomington, IN, USA. [9] Centre for Eudaimonia and Human Flourishing, Linacre College, University of Oxford, Oxford, UK. [10] Department of Psychiatry, University of Oxford, Oxford, UK. [11] Center for Music in the Brain, Department of Clinical Medicine, Aarhus University, Aarhus, Denmark. ✉email: gustavo. deco@upf.edu; morten.kringelbach@psych.ox.ac.uk

The biophysics of the brain shows surprisingly slow information transfer between neurons, the brain's fundamental computational units. Starting with the Nobel prizewinning research of Hodgkin and Huxley[1], researchers have meticulously demonstrated that information transfer between neurons is slow with cortical latencies of around 10–20 ms[2], arising from the fact that the electrical signals in the myelinated fibres have to be converted to a chemical signal at the synaptic junction and back to electrical signal[3]. This slow process poses significant challenges in terms of how the brain manages to solve the difficult computational problems necessary for survival. Paradoxically, however, the wetware of brain is often much better at solving problems than the much faster silicon-based computers. This raises the unsolved physical problem of how the brain overcomes the limitations of speed for information transfer across spacetime.

Here we propose that efficient information transfer across the whole brain depends on turbulence, and we demonstrate turbulence in fast neuronal brain dynamics directly measured with magnetoencephalography. Originally coined "turbolenza" by Leonardo DaVinci over 500 years ago[4], turbulence has shown to be ubiquitous in nature as an essential dynamical regime facilitating energy and efficient information transfer across spatiotemporal scales[5]. The spatial power scaling law is a hallmark of turbulence[6,7], revealing the underlying key mechanisms of fluid dynamics, namely the energy cascades that balance kinetics and viscous dissipation. Turbulence is not, however, limited to fluids but also found in many other physical systems including coupled oscillators[8]. This has been used to show turbulence in the brain in signals from functional magnetic resonance (fMRI)[9,10], demonstrating the existence of a similar power law in the turbulent core, similar to the 'inertial subrange' found in fluid dynamics, and which similarly appear to be homogeneous isotropic, i.e. with average properties that are both independent of position and direction. This strongly suggest the presence of a cascade of efficient information processing across scales.

Further bolstering these findings, we have also showed that the brain is turbulent using a measure from the theory of coupled oscillators, namely the 'local metastability' measure proposed by Kuramoto and colleagues. This extends the very important research carried out by Kuramoto, showing that coupled oscillators can be used to capture turbulence in many other systems[8]. The Stuart-Landau model of a single oscillator provides the simplest non-linear extension of a linear oscillator that mathematically describes the onset of spontaneous oscillations (i.e. bifurcation from fixed-point dynamics towards a limit cycle), which has been used to model many physical systems, going from the simplest linear, harmonic oscillator to non-linear oscillators[11]. Changes in oscillation amplitudes can be brought about by small perturbations to linear oscillators, while small perturbations to non-linear oscillators, such as the Stuart-Landau oscillator, lead to self-regulating relaxation and return to the same region in phase space. This is highly convenient given that the dynamics of the brain can be described by a whole-brain model of coupled oscillators[9,12], using the *Hopf whole-brain model*, named in honour of the German mathematician Eberhard Hopf who described the normal form of the Hopf bifurcation, which describes the behaviour of a Stuart-Landau non-linear oscillating system[13]. In neuroscience, the Hopf whole-brain model has been shown to be remarkably effective at modelling the mesoscopic dynamics of brain regions and capture the regularities of empirical neuroimaging data[12,14,15], as well for modelling the turbulence found in fMRI dynamics[4,9,10,16].

Specifically, within the framework of coupled oscillators, turbulence can be characterised as the variability across space and time of the 'local metastability', which measures the local level of synchronisation of the coupled oscillators[9,10]. This characterisation is a generalisation of the concept of metastability[17–21], which has been used in neuroscience to measure the variability across time of the *global* level of synchronisation of the whole system, commonly known as the global Kuramoto order parameter of a dynamical system. This suggest that the turbulent regime with its underlying coupled oscillators could sustain optimal information transmission[22].

This, however, poses the outstanding problem of whether turbulence is also found in fast *whole-brain* dynamics. Previous research has demonstrated turbulence in the fast dynamics of *local* neuronal circuits[23] but showing turbulence in fast *global* brain dynamics is a crucial step, which has not been answered by the previous research using fMRI which is both relatively slow with a timescale of seconds due to haemodynamic response[24] and not directly measuring neural dynamics. To solve this problem, we used MEG, a neuroimaging modality directly measuring fast neuronal dynamics at the whole-brain level[25]. However, we needed to overcome the problem that MEG has less good spatial resolution than fMRI, which means that we cannot use the existing method for demonstrating turbulence, which requires high spatial resolution using a fine parcellation of around 1000 regions.

In order to solve this problem, here we propose an 'edge metastability' measure to overcome these challenging physical spatiotemporal problems and detect turbulence in fast brain dynamics. As the name suggests, this method relies on using the spatiotemporal variability of edge time series, recently introduced to capture fine-scale dynamics in fMRI recordings[26–28]. In contrast to existing methods, this method can capture turbulence with high temporal precision in a coarse-grained ring of coupled oscillators, where the level of turbulence can be exactly analytically determined[22].

Results

First, we tested our measure in a ring of Stuart-Landau (SL) oscillators with non-local coupling (Fig. 1a), where, crucially, there is a known analytical solution to where the turbulent regime is found[22] (see Methods for the equations governing this system). Then we tested this measure in empirical MEG data (see Methods for details on empirical data) to demonstrate the existence of turbulence.

Results using ring model. We studied empirical measurements of turbulence for different levels of coarse-graining in a ring of SL oscillators. First, we performed simulations of this ring using $n_{org} = 10,000$ oscillators (Fig. 1b). The fine parcellation corresponds to observations of the phase dynamics at this level, while the coarse parcellation (Fig. 1c) is divided into groups of $n_{obs} = 100$ neighbouring SL oscillators to emulate the natural coarse-graining obtained with MEG, and use the mean of the phase in these oscillators. Fig. 1d shows an example of the temporal evolution of the phases of the coarse parcellation in the maximal point of the turbulent regime ($D = 0.0524$, see below), which is given by the analytical solution for this system provided by Kawamura and colleagues[22] (see Methods).

Fig. 1e shows the bifurcation diagram for the analytical analysis. Here, the blue curve represents the border between the oscillatory and turbulent regimes, while the red line represents the Hopf bifurcation curve, and the green line the well-known Benjamin-Feir criticality, which is a hallmark of the complex Ginzburg-Landau equation. Specifically, the Benjamin-Feir criticality line demarcates the transition to turbulence, given that the spatially uniform oscillation of the complex Ginzburg-Landau equation becomes unstable and spatiotemporal chaos develops when the Benjamin-Feir instability condition is satisfied.
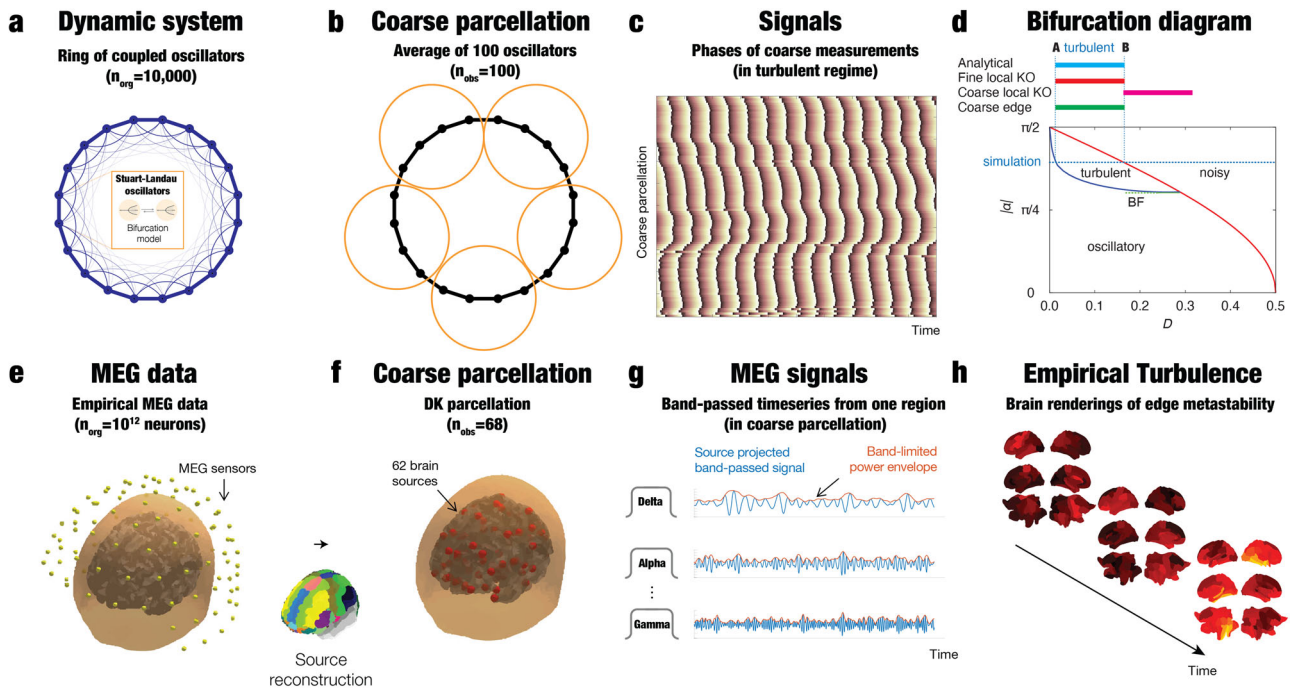
Fig. 1 Edge metastability measure of turbulence. a Validation of turbulence measure in a ring of Stuart-Landau (SL) oscillators with non-local coupling (first panel), where, crucially, there is a known analytical solution to where the turbulent regime is found. **b** The panel shows how we constructed the spatially coarse observations by averaging over 100 neighbouring oscillators. **c** The panel shows an example of the phases of these coarse measurements for simulations in the turbulent regime. **d** The panel shows the bifurcation diagram for the analytical analysis and the performance of the different measures of turbulence. **e** The pipeline of pre-processing MEG data shows the sensor signals. **f** These signales are beamformed and a coarse DK68 parcellation was used to extract the MEG signals. **g** The panel shows examples from each coarse parcel in the five classical bands (delta 1-3 Hz, theta 3.5-7 Hz, alpha 7.5-13.5 Hz, beta 14–30.5 Hz, gamma 31–40 Hz). **h** The panel shows examples of the measures of empirical turbulence on representative successive timepoints are rendered on sideways, midline and flat map renderings of the whole brain.

The stippled blue line represents the results of running the simulation with $\alpha = 1.2036$, i.e., $\beta = 2.6$. This allows us to identify two points, A and B, which demarcates the transition from the oscillatory to turbulent and turbulent to noisy regimes, respectively. Point A is found at D = 0.025 and point B is found at D = 0.18. Given that we know the ground truth for the turbulent regime in these simulations, we can check our measures of turbulence against this analytical solution (shown by the solid blue bar at the top of bifurcation diagram).

We first tested the standard empirical measure of turbulence[22] (using the local Kuramoto order parameter, Eq. (6) in Methods). In Fig. 1d, the solid red bar shows that using this measure on the fine parcellation ($n_{org} = 10,000$) perfectly identifies the turbulent regime since Wilcoxon significance tests show that only in this region the measure is larger than in the oscillatory and noisy regions ($p < 0.001$). On the other hand, when this measure is used on the coarse parcellation ($n_{obs} = 100$), it fails (see solid pink bar).

In order to be able to empirically measure turbulence in the coarse parcellation we introduce a definition of edge metastability, which has not appeared in the literature before (Eq. (7) in the Methods).

When applied to the coarse parcellation, this measure perfectly identifies the turbulent regime given that Wilcoxon significance tests show that only in this region the measure is larger than in the oscillatory and noisy regions ($p < 0.001$). This is shown by the solid green bar above bifurcation diagram in Fig. 1d.

Further investigating these and related measures, they were applied to four points as shown in Fig. 2. The first point is placed deep in the oscillatory regime ($D = 0.0011$). The second and third point are placed in the turbulent regime with one at the

maximum of turbulence ($D = 0.0524$), while the other is in the turbulent region but close to the edge of the noisy regime ($D = 0.1671$). Finally, the fourth point is in the noisy regime at the edge of turbulence ($D = 0.1805$).

Fig. 2a shows the boxplots for these four points (across 100 trials) using the mean value across time of the global Kuramoto order parameter R_G (see Eq. (8) in Methods). Fig. 2b shows the boxplots of using global metastability, i.e., the standard deviation across time of the global Kuramoto order parameter. As can be seen, both measures are unable to detect turbulence. In contrast, as already shown in Fig. 1d, Fig. 2c shows the boxplots at the four points using the spatiotemporal metastability at the fine parcellation. This measure closely tracks the presence of turbulence since it is significantly higher in the turbulent regime compared to the oscillatory and noisy regimes. Yet, when applied to the coarse parcellation, Fig. 2d shows that this measure fails to significantly detect turbulence.

For reference, Fig. 2e, f show the spacetime evolution in specific trials of the simulation of R and snapshots of the phases, respectively. Note how the two middle panels clearly indicate the presence of turbulence, reflecting the vorticity of the local synchronization.

We then demonstrate, as shown in Fig. 2g, that the measure of edge metastability is able to perfectly capture the turbulent regime. The added inset shows a close-up of the last three boxplots across the 100 trials.

Further, we defined the Edge Spacetime Predictability (ESP) as the information transfer correlation across space and time by computing the predictability of the edge measure over space and time (see Eq. 9 in Methods). This allowed to demonstrate the efficiency of information transfer in the turbulent regime. Fig. 2h
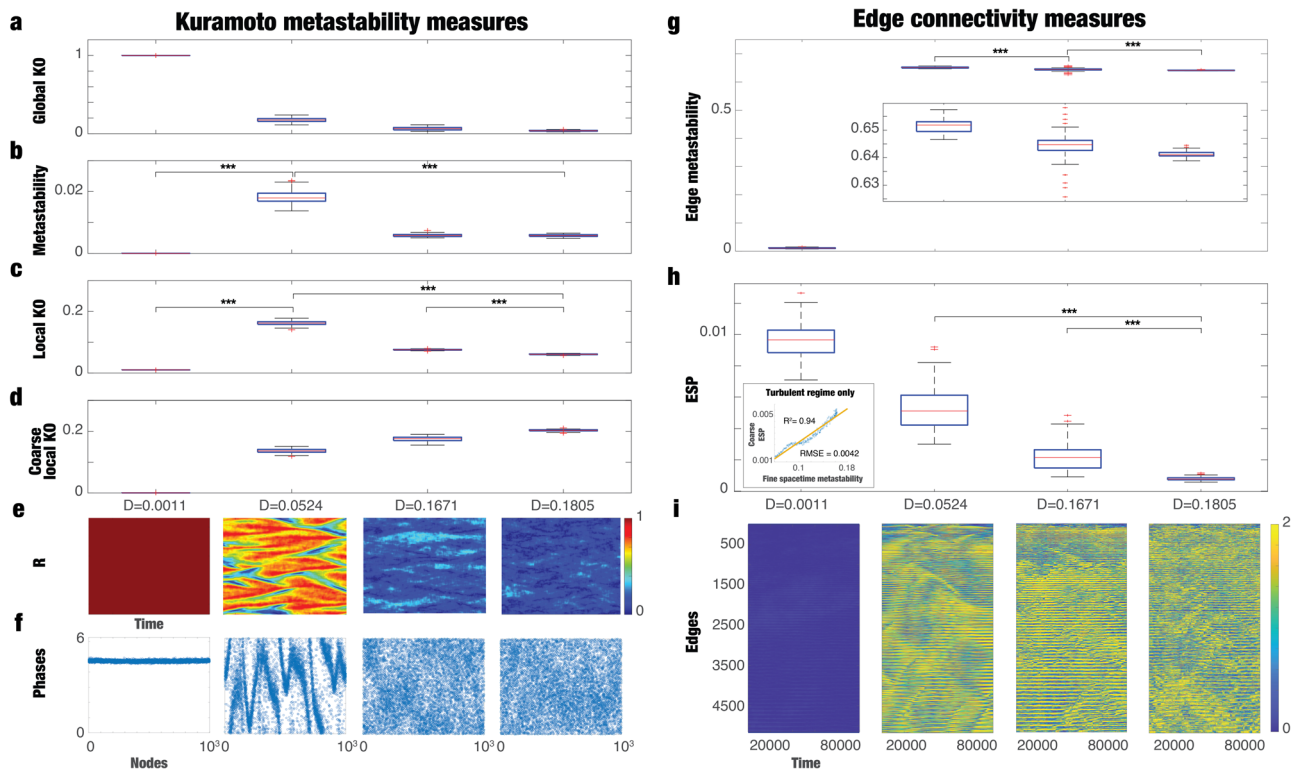
Fig. 2 Validation of an empirical measure of turbulence in a ring of coupled oscillators. The figure demonstrated the suitability of different measures for capturing turbulence by using the same four points, where the first ($D = 0.0011$) is deep in the oscillatory regime, the second is at the maximum of turbulence ($D = 0.0524$), the third is in the turbulent region but close to the edge of the noisy regime ($D = 0.1671$), while the fourth point is in the noisy regime at the edge of turbulence ($D = 0.1805$). **a** The mean value across time of the global Kuramoto order parameter is not sensitive as shown from the boxplots (across 100 trials). **b** Equally, global metastability is not able to capture turbulence. **c** In contrast, spatiotemporal metastability at the fine spatial scale detect turbulence perfectly. **d** However, using this measure at the coarse spatial scale fails to significantly detect turbulence. **e** Examples of the spacetime evolution in specific trials of the simulation of R, where the two middle panels clearly show turbulence, reflecting the vorticity of the local synchronisation. **f** Spacetime evolution snapshots of the phases. **g** The measure of edge metastability perfectly captures the turbulent regime using only coarse spatial observations, as shown in detail in the magnified inset showing a close up of the last three boxplots across the 100 trials. **h** The measure of Edge Spacetime Predictability (ESP) characterises the information transfer correlation across space and time and shows significant differences between the turbulent and noisy regimes. Furthermore, the inset shows the correlation in the turbulent regime between the fine spacetime metastability and the coarse ESP. **i** Examples of the evolution in time of the edge metastability for one trial at each of the four timepoints. The error bars depict the standard error.

shows the significant differences for this measure between the turbulent and noisy regimes. Furthermore, the inset shows the scatterplot in the turbulent regime between the fine spacetime metastability and the coarse ESP, demonstrating the increase of information transfer with the level of turbulence.

For illustration, Fig. 2i shows the evolution in time of the edge metastability for one trial at each of the four timepoints. Note how the second panel (at the peak of turbulence) shows a rich edge metastability repertoire.

Results for empirical MEG data. Overall, these results used on the ring model with a known true turbulent regime clearly demonstrate the usefulness of our edge metastability measure for detecting turbulence from coarse spatial observations. This provided us with the impetus to use this measure to detect turbulence in spatially coarse but temporally fine MEG resting-state data data from 89 participants from the openly available Human Connectome Project. Fig. 1e–g show the pipeline of preprocessing MEG data, which takes the sensor signals, beamform these and use a coarse DK68 parcellation[29] to extract the MEG signal from each coarse parcel in the five classical bands (delta 1–3 Hz, theta 3.5–7 Hz, alpha 7.5–13.5 Hz, beta 14–30.5 Hz, gamma 31–40 Hz) (see "Methods" for details). Please note that due to constraints in the beamforming technique, it is not

possible to spatially reconstruct the signal at more than between 60 and 90 parcels. As shown in Fig. 1h, the empirical edge metastability turbulence can then be visualised for successive timepoints on lateral, midline and flat map renderings of the whole brain.

For applying our edge metastability measure to MEG data, which consists of broadband amplitude signals, we used the standard definition of edge-centric used in fMRI[26–28] (see Eq. 10 in the Methods).

As shown by the ring model simulations (where the ground truth is known), the crucial issue for detecting turbulence is to use the right reference regime, i.e. compare measures of turbulence (local metastability and edge-centric metastability) in a turbulent regime with a non-turbulent regime. While there is redundancy in both turbulent and non-turbulent regimes, both measures can detect the difference in turbulence even if highly redundant such as the measure of edge-centric metastability. For the empirical study, we compare this measure on both the empirical MEG and surrogate data.

The results clearly show the existence of turbulence for all bands (see Fig. 3a) compared to circular shifted surrogate data[30,31]. In brief, this method generates 89 independent circular time-shifted surrogates by separately resampling the signal for each of the 89 participants. Specifically, for each timeseries of each parcel, one independent random integers c is randomly
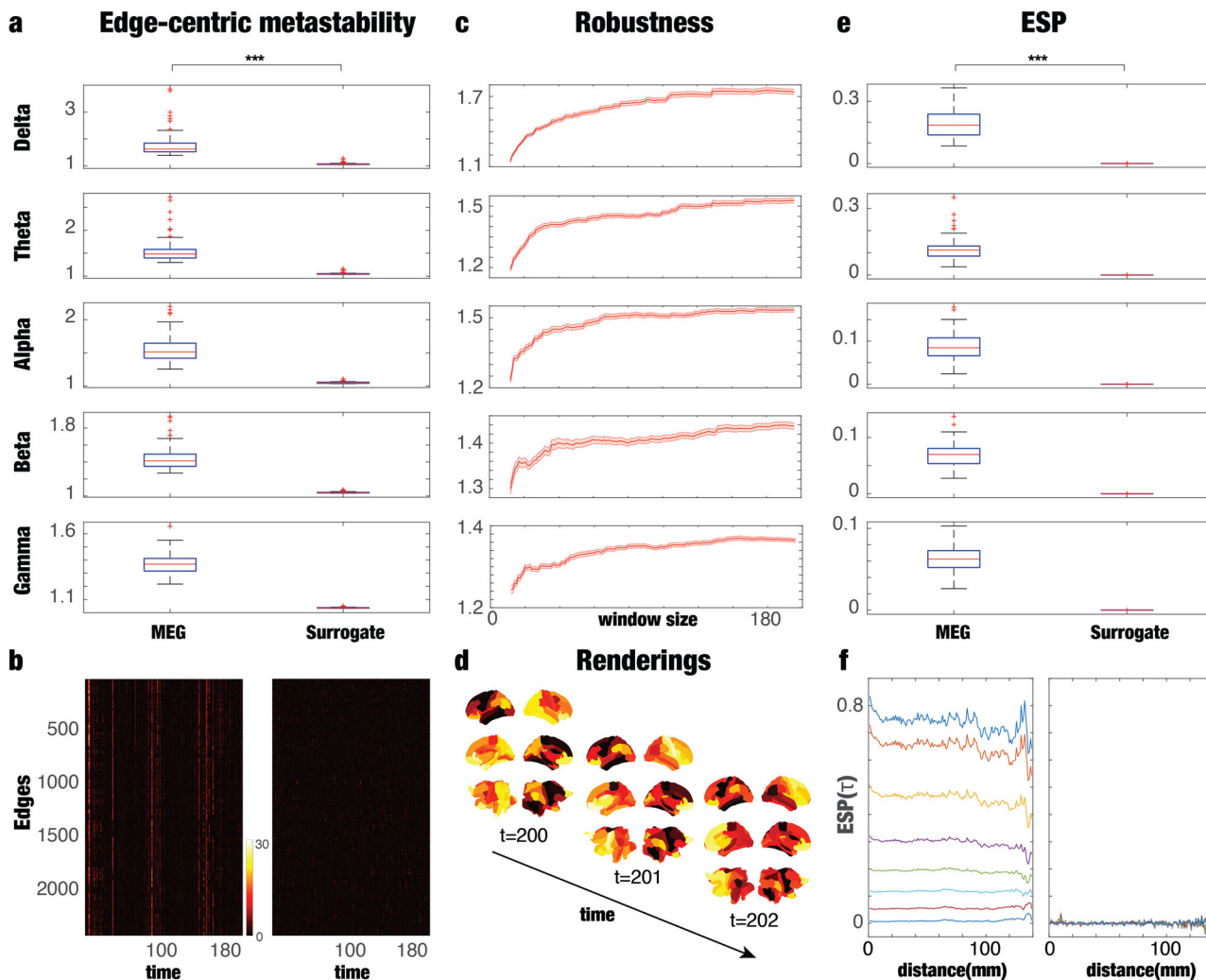
Fig. 3 Turbulence in fast, neuronal whole-brain dynamics measured with magnetoencephalography (MEG) in human participants. a The measure of edge-centric metastability shows clear turbulence for all five bands of MEG data compared to circular shifted surrogate data. **b** An example of the edge matrix for 200 data points the MEG data of one participant and for the corresponding surrogate data. **c** The robustness of the edge-centric metastability is demonstrated by the asymptotic behaviour of the average of the edge-centric metastability as a function of the length of the MEG data time series. The figure shows this asymptotic behaviour for all five bands with the shadow reflecting the standard error. **d** Visualisations for a single participant of the edge turbulence for the delta band for three successive timepoints rendered on 3D views (sideways and midline) as well as flat map renderings of the whole brain. **e** Using measure of Edge Spacetime Predictability (ESP) on MEG data (compared with surrogate data), shows significant differences for all five bands, suggesting the efficiency of the turbulent regime for information transfer. **f** An example for the delta band in a specific participant of the evolution of the seven different predictions (different coloured curves, $\tau = [1..7]$ in Eq. 9) as function of the Euclidean distance between parcels (x-axis). The error bars depict the standard error.

generated within the interval [0.05n 0.95n] (where n is the number of time points in the time series signal). Then the circular time-shift is performed by moving the first c values of $X = [X_1, \ldots, X_n]$ to the end of the time series which creates the surrogate sample $X = [X_{c+1}, \ldots, X_n, X_1, \ldots, X_c]$. This type of surrogates does not assume Gaussianity and has been shown to preserve the whole statistical structure of the original time series. In Fig. 3b, we show an example of the edge matrix for 200 data points derived from the MEG data of one participant and for the corresponding surrogate data. There is clearly structure in the edge matrix for MEG and not for the surrogate.

Figure 3c shows the reliability and the robustness of the edge-centric metastability by plotting the average of the edge-centric metastability as a function of the length of the MEG data time series. The asymptotic behaviour found for all five bands clearly demonstrates the robustness of the measure for a time series

larger than around 140 seconds, when the edge-centric metastability is converging on the value for the full time series.

Figure 3d shows visualisations for a single participant of the edge turbulence for the five different bands for successive timepoints rendered on sideways, midline and flat map renderings of the whole brain.

Figure 3e shows the ESP measure on the MEG data (compared with surrogate data) and demonstrates significant differences for all bands. Figure 3f shows an example for the delta band in a specific participant of the evolution of the seven different predictions (different coloured curves, $\tau = [1..7]$ in Eq. 9, see Methods) as function of the Euclidean distance between parcels (x-axis). Applying ESP to the MEG data shows clear spacetime predictability, while applying this to the surrogate data shows no predictability. This suggests the efficiency of the turbulent regime for information transfer.

Conclusions

Overall, here we created and validated a measure of turbulence suitable for spatially coarse observations in the well-controlled environment of a ring of coupled SL oscillators. This allowed us to demonstrate turbulence in the fast brain neuronal dynamics measured with MEG in a large group of human participants.

The present findings of turbulence in MEG data include only cortical regions similar to the previous findings of turbulence in fMRI[4,9,10,16]. It would be of considerable interest to include subcortical regions but this poses unique challenges for MEG given the challenges of the source reconstruction from deep sources[32]. We expect that subcortical regions will also contribute to the generation of turbulence given the findings of Maurer and colleagues of turbulence in the rodent local field potential recordings from the hippocampus[23]. It would also be of considerable interest to apply the present measure of turbulence to such data.

We also showed efficient information transmission across the whole brain in the turbulent regime. This provides further insight into how turbulence is the skeleton underlying efficient spatiotemporal information transfer required for survival. This measure is an excellent candidate for having the specificity and sensitivity for differentiating between different brain states as for example wakefulness, sleep, cognitive tasks (for example, decision making and working memory), drugs (anaesthesia and psychedelics) and disease (coma and neuropsychiatric disorders). The measure should also be useful for identifying moments of high information transfer/turbulence in extended time series, individual differences, and differences between normal and clinical populations.

Methods and experimental data

Modelling of non-local coupled oscillators in ring structure. First, we tested this measure in a ring of Stuart-Landau (SL) oscillators with non-local coupling, where, crucially, there is a known analytical solution to where the turbulent regime is found[22]. This system can be described by the following equations:

$$\partial_t W(x,t) = (1 + i\omega_0)W - (1 + i\beta)|W|^2 W + KS_W(x,t) + \sqrt{\sigma}\eta_W(x,t) \quad (1)$$

and

$$S_W(x,t) = \int_{-\infty}^{\infty} dx' G(x - x')W(x',t) \quad (2)$$

The nonlocal coupling, G, is given by $G(x) = 0.5e^{-|x|}$. Derived as a normal form of the supercritical Hopf bifurcation, the SL oscillator is the simplest limit-cycle oscillator[8]. Each oscillator state is here described by a complex amplitude, W, and where the coupling term S_W and the noise η_W are also complex variables. The parameters β and σ are controlled by the parameters $\omega_0 = \beta + 1.0$ and $K = 0.05$. The values of the parameter β was chosen in such a way that the spatially uniform oscillation is stable and the system is nonturbulent in the absence of noise[22].

As shown by Kuramoto and colleagues[8,22], for the Stuart-Landau oscillator, mapping from the complex amplitude W to the generalized phase is analytically given as

$$\phi = \arg W - \beta \ln|W| \quad (3)$$

Analytical solution to ring model. Applying the standard phase reduction method to this system allowed Kuramoto and colleagues to derive an approximate equation consisting of only the phase variable from the original dynamical equations in multiple variables, given by

$$\partial_t \phi(x,t) = \widetilde{\omega} - K\sqrt{1 + \beta^2} \int_{-\infty}^{\infty} dx' G(x - x')\sin\left[\phi(x,t) - \phi'(x',t) + \alpha\right] + \sqrt{\widetilde{D}}\xi(x,t) \quad (4)$$

where the natural frequency $\widetilde{\omega} = \omega_0 - \beta$, the effective noise intensity $\widetilde{D} = \sigma(1 + \beta^2)$ and $\alpha = \arg(1 + i\beta)$. The noise $\xi(x,t)$ is a real scalar spatiotemporally white Gaussian noise satisfying

$$\langle \xi(x,t) \rangle = 0, \langle \xi(x,t)\xi(x',t') \rangle = 2\delta(x - x')\delta(t - t').$$

Furthermore, the equation can be simplified by changing the time scale, yielding

$$\partial_t \phi(x,t) = \omega - \int_{-\infty}^{\infty} dx' G(x - x')\sin\left[\phi(x,t) - \phi(x',t) + \alpha\right] + \sqrt{D}\xi(x,t) \quad (5)$$

where the rescaled noise intensity is given by $D = \frac{\sigma\sqrt{1+\beta^2}}{K}$. The analytical solution is obtained by transforming the Langevin phase equation to an equivalent Fokker Planck equation - for details consult Kawamura and colleagues[22].

Defining spatiotemporal metastability. We extended the standard empirical measure of turbulence[22], spatiotemporal metastability, namely the variability across spacetime of the local Kuramoto order parameter R given by:

$$R(x,t)e^{i\Theta(x,t)} = \int_{-\infty}^{\infty} dx' G(x - x')e^{i\phi(x',t)} \quad (6)$$

Definition of edge metastability. In order to be able to empirically measure turbulence in the coarse parcellation we introduce a definition of edge metastability, which is the standard deviation of the edge centred matrix E, which is defined as follows. Each column corresponds to a timepoint t, where the column is defined as vector combining all pairwise combinations of the differences of the phases' state at time t. With N parcels this results in $\frac{N(N-1)}{2}$ pairs. The difference of the phase state at a given timepoint t for the different pairs are given by

$$E_{i,j}(t) = \sqrt{\left(\cos(\phi_i(t)) - \cos(\phi_j(t))\right)^2 + \left(\sin(\phi_i(t)) - \sin(\phi_j(t))\right)^2} \quad (7)$$

Where i,j are the parcels in a given parcellation. In other words, the edge metastability is the standard deviation across space and time of the edge-centric measure.

The global Kuramoto order parameter. The global Kuramoto order parameter R_G is defined according to

$$R_G(t)e^{i\Theta_G(t)} = \int_{-\infty}^{\infty} dx' e^{i\phi(x',t)} \quad (8)$$

Edge Spacetime Predictability (ESP). The Edge Spacetime Predictability (ESP) is defined as the information transfer correlation across space and time by computing the predictability of the edge measure over space and time. ESP is defined as the mean value over all pairs of the mean value of the shifted correlations across time shift $\tau = [1..7]$. For each pair i,j the shifted correlation for a given τ is defined as

$$C_{i,j}(\tau) = \frac{\sum_t \widetilde{E}_{i,j}(t - \tau)\widetilde{E}_{i,j}(t)}{\sqrt{\widetilde{E}_{i,j}(t - \tau)^2}\sqrt{\widetilde{E}_{i,j}(t)^2}} \quad (9)$$

Where $\widetilde{E}_{i,j}$ is the de-meaned version of $E_{i,j}$.

Ethics for experimental data. The Washington University–University of Minnesota (WU-Minn HCP) Consortium obtained full informed consent from all participants, and research procedures and ethical guidelines were followed in accordance with Washington University institutional review board approval (Mapping the Human Connectome: Structure, Function, and Heritability; IRB # 201204036).

Neuroimaging acquisition for MEG HCP. We used the human non-invasive resting state magnetoencephalography (MEG) data publicly available from the Human Connectome Project (HCP) consortium, acquired on a Magnes 3600 MEG (4D NeuroImaging, San Diego, USA) with 248 magnetometers. The resting state data consist of 89 participants (mean 28.7 years, range 22–35, 41 f / 48 m, acquired in 3 subsequent sessions, lasting 6 min each).

Preprocessing and extraction of MEG data timeseries. For each participant, the MEG data were acquired in a single continuous run comprising resting state. As a starting point we used the preprocessed MEG data from the HCP database. At this level of preprocessing, removal of artefactual independent components, bad samples and channels has already been performed. Following the preprocessing pipeline detailed in ref. [33], MEG data were then downsampled to 250 Hz using an anti-aliasing filter, filtered out frequencies below 1 Hz, performed the co-registration with the head models provided by the HCP, and source-reconstructed using LCMV beamforming[32] to the 68 cortical regions of the Desikan-Kahilly parcellation[29]. For each region, a single time series was computed as the first principal component of the voxels within that parcel. Each region's time series was then standardized to have mean equal zero and standard deviation equal one, so that the amount of variance was always the same regardless of the depth of the region. In order to project the results to brain space, we used a weighted mask, where each region had its maximum value at the centre of gravity.

Measuring turbulence in MEG analysis. For applying our edge metastability from the ring model to MEG data, which consists of broadband amplitude signals, we used the standard definition of edge-centric used in fMRI:[26–28]

$$E_{i,j}(t) = Z_i(t)Z_j(t) \qquad (10)$$

Where Z is the z-scored Hilbert envelope of the filtered MEG signals. Please note that Eq. (10) differs from Eq. (7), in that this equation uses the Hilbert envelopes of the empirical signals rather than the phases which are explicitly given by the ring simulation but not in the empirical data. Much of the current MEG analysis is based on using envelopes[21,34,35], and we therefore preferred to use Eq. (10) when analysing the MEG data. However, we did also compute the phase version for the MEG data and the results were qualitatively identical.

Reporting summary. Further information on research design is available in the Nature Portfolio Reporting Summary linked to this article.

Data availability

The multimodal neuroimaging data are freely available from HCP: https://www.humanconnectome.org/.

Code availability

The code used to run the analysis from the HCP data is available on GitHub (https://github.com/decolab/megturbulence).

References

1. Hodgkin, A. L. & Huxley, A. F. A quantitative description of membrane current and its application to conduction and excitation in nerve. *J. Physiol. (Lond.)* **117**, 500–544 (1952).
2. Itoh, K. et al. Cerebral cortical processing time is elongated in human brain evolution. *Sci. Rep.* **12**, 1103 (2022).
3. Cotterill, R. M. J. *Biophysics. An Introduction* (Wiley, 2002).
4. Deco, G., Kemp, M. & Kringelbach, M. L. Leonardo da Vinci and the search for order in neuroscience. *Curr. Biol.* **31**, R704–R709 (2021).
5. Cross, M. C. & Hohenberg, P. C. Pattern formation outside of equilibrium. *Rev. Mod. Phys.* **65**, 851–1112 (1993).
6. Kolmogorov, A. N. The local structure of turbulence in incompressible viscous fluid for very large Reynolds numbers. *Proc. USSR Acad. Sci. (Atmos. Ocean. Phys.)* **30**, 299–303 (1941).
7. Kolmogorov, A. N. Dissipation of energy in locally isotropic turbulence. *Proc. USSR Acad. Sci. (Russian)* **32**, 16–18 (1941).
8. Kuramoto, Y. *Chemical Oscillations, Waves, and Turbulence.* (Springer-Verlag, 1984).
9. Deco, G. & Kringelbach, M. L. Turbulent-like dynamics in the human brain. *Cell Rep.* **33**, 108471 (2020).
10. Deco, G. et al. Rare long-range cortical connections enhance human information processing. *Curr. Biol.* **31**, 1–13 (2021).
11. García-Morales, V. & Krischer, K. The complex Ginzburg–Landau equation: an introduction. *Contemp. Phys.* **53**, 79–95 (2012).
12. Deco, G., Kringelbach, M. L., Jirsa, V. & Ritter, P. The dynamics of resting fluctuations in the brain: metastability and its dynamical core [bioRxiv 065284]. *Sci. Rep.* **7**, 3095 (2017).
13. Hopf, E. Abzweigung einer periodischen Lösung von einer stationären Lösung eines Differentialsystems. *Ber. Verh. Sächs. Akad. Wiss. Leipz., Math. -Nat. Kl.* **94**, 3–22 (1942).
14. Deco, G. et al. Awakening: predicting external stimulation forcing transitions between different brain states. *PNAS* **116**, 18088–18097 (2019).
15. Kringelbach, M. L. & Deco, G. Brain states and transitions: insights from computational neuroscience. *Cell Rep.* **32**, 108128 (2020).
16. Escrichs, A. et al. Unifying turbulent dynamics framework distinguishes different brain states. *Commun. Biol.* **5**, 638 (2022).
17. Tognoli, E. & Kelso, J. A. The metastable brain. *Neuron* **81**, 35–48 (2014).
18. Wildie, M. & Shanahan, M. Metastability and chimera states in modular delay and pulse-coupled oscillator networks. *Chaos* **22**, 043131 (2012).
19. Shanahan, M. Metastable chimera states in community-structured oscillator networks. *Chaos* **20**, 013108 (2010).
20. Kitzbichler, M. G., Smith, M. L., Christensen, S. R. & Bullmore, E. Broadband criticality of human brain network synchronization. *PLoS Comput. Biol.* **5**, e1000314 (2009).
21. Cabral, J. et al. Exploring mechanisms of spontaneous functional connectivity in MEG: How delayed network interactions lead to structured amplitude envelopes of band-pass filtered oscillations. *Neuroimage* **90**, 423–435 (2014).
22. Kawamura, Y., Nakao, H. & Kuramoto, Y. Noise-induced turbulence in nonlocally coupled oscillators. *Phys. Rev. E, Stat., nonlinear, soft matter Phys.* **75**, 036209 (2007).
23. Sheremet, A., Qin, Y., Kennedy, J. P., Zhou, Y. & Maurer, A. P. Wave turbulence and energy cascade in the hippocampus. *Front. Syst. Neurosci.* **12**, 62 (2019).
24. Kwong, K. K. et al. Dynamic magnetic resonance imaging of human brain activity during primary sensory stimulation. *Proc. Natl Acad. Sci. USA* **89**, 5675–5679 (1992).
25. Hansen, P. C., Kringelbach, M. L. & Salmelin, R. *MEG. An Introduction To Methods* (Oxford University Press, 2010).
26. Faskowitz, J., Esfahlani, F. Z., Jo, Y., Sporns, O. & Betzel, R. F. Edge-centric functional network representations of human cerebral cortex reveal overlapping system-level architecture. *Nat. Neurosci.* **23**, 1644–1654 (2020).
27. Sporns, O., Faskowitz, J., Teixeira, A. S., Cutts, S. A. & Betzel, R. F. Dynamic expression of brain functional systems disclosed by fine-scale analysis of edge time series. *Netw. Neurosci.* **5**, 405–433 (2021).
28. Zamani Esfahlani, F. et al. High-amplitude cofluctuations in cortical activity drive functional connectivity. *Proc. Natl Acad. Sci. USA* **117**, 28393–28401 (2020).
29. Desikan, R. S. et al. An automated labeling system for subdividing the human cerebral cortex on MRI scans into gyral based regions of interest. *NeuroImage* **31**, 968–980 (2006).

30. Quiroga, R. Q., Kraskov, A., Kreuz, T. & Grassberger, P. Performance of different synchronization measures in real data: a case study on electroencephalographic signals. *Phys. Rev. E* **65**, 041903 (2002).
31. Deco, G., Vidaurre, D. & Kringelbach, M. L. Revisiting the Global Workspace orchestrating the hierarchical organisation of the human brain. *Nat. Hum. Behav.* **5**, 497–511 (2021).
32. Hillebrand, A. & Barnes, G. R. Beamformer analysis of MEG data. *Int Rev. Neurobiol.* **68**, 149–171 (2005).
33. Vidaurre, D. et al. Spontaneous cortical activity transiently organises into frequency specific phase-coupling networks. *Nat. Commun.* **9**, 2987 (2018).
34. Brookes, M. J. et al. Measuring functional connectivity using MEG: methodology and comparison with fcMRI. *NeuroImage* **56**, 1082–1104 (2011).
35. Hipp, J. F., Hawellek, D. J., Corbetta, M., Siegel, M. & Engel, A. K. Large-scale cortical correlation structure of spontaneous oscillatory activity. *Nat. Neurosci.* **15**, 884–890 (2012).

Author contributions

G.D. and M.L.K. designed the study, developed the methods and wrote the manuscript. Y.S.P, S.L.G. and O.S. contributed methods. All the authors edited the manuscript.

Competing interests

The authors declare no competing interests.

Additional information

Supplementary information The online version contains supplementary material available at https://doi.org/10.1038/s42005-023-01192-2.

Correspondence and requests for materials should be addressed to Gustavo Deco or Morten L. Kringelbach.

Peer review information *Communications Physics* thanks Yingying Wang and the other, anonymous, reviewer(s) for their contribution to the peer review of this work.

Reprints and permission information is available at http://www.nature.com/reprints

Publisher's note Springer Nature remains neutral with regard to jurisdictional claims in published maps and institutional affiliations.